Aeroelastic Tailoring of Aft–Swept High Aspect Ratio Composite Wings

John A Green*
Stanford University
Stanford, CA

ICAS-86-4.8.4

Abstract

The effects of several geometric and aerodynamic parameters on the aeroelastic stability of aft–swept high aspect ratio composite wings are studied. The solution procedure is based on an integrating matrix method, which is a relatively fast numerical procedure. The method does require the wing to be discretised, though not to the same extent as in a finite element formulation, and this allows arbitrary geometries to be investigated. Results are presented to demonstrate some of the effects of wing geometry, and the potential of non–symmetric composite laminates is evaluated. It is shown that there need not be a severe aeroelastic penalty for using such general laminates.

Nomenclature

A_{ij}, a_{ij} Extensional modulus/compliance.

$A.R.$ Aspect ratio.

$a.c.$ Location of aerodynamic centre in semi–chords, positive aft of mid–chord.

B_{ij}, b_{ij} Non–symmetric coupling modulus/compliance.

B Boundary condition matrix.

b_0^T, b_n^T Boundary condition vectors.

b_R Structural semi–chord.

$C_{l\alpha}$ Lift curve slope.

c_R Aerodynamic chord.

D_{ij}, d_{ij} Bending modulus/compliance.

e Location of structural axis in semi–chords, positive aft of mid–chord.

k Constant of integration vector.

L Integrating Matrix.

l Semi–span.

M Mass matrix.

M_s, M_{sy} Dimensionless bending moments.

M_α, M_w, M_γ Dimensionless aerodynamic moments.

$m_{i,j}$ Mass terms, non–dimensionalised by m_R.

m_R Mass per unit length at root.

S Summing matrix.

s Laplace variable.

V_s Dimensionless transverse shear force.

W_n Weighting matrix of order n.

w Vertical displacement.

x Dimensionless spanwise coordinate.

y Dimensionless chordwise coordinate.

Z Matrix of dimensionless structural compliances.

Q Aerodynamic matrix.

Q_{ij} Transformed modulus.

q Dimensionless dynamic pressure.

R Dimensionless bending–torsion ratio.

r_α Dimensionless radius of gyration.

Greek Symbols

α Angle of attack.

γ Bending rotation angle.

θ Laminate ply orientation angle.

Λ Sweep angle.

μ Mass ratio $(m_R/\pi\rho b_R^2)$.

τ Taper ratio, c_t/c_r.

χ_α Dimensionless static unbalance relative to strucural axis, positve aft.

ψ, ψ_i Dimensionless coupling parameters.

Sub– and Superscripts

$()_D$ Displacement variable.

$()_F$ Force variable.

$()_S$ Symmetric.

$()_T$ Total laminate.

$()_U$ Unsymmetric.

$\hat{()}$ Global matrix or vector.

$()'$ Derivative with respect to x.

* Research Assistant, Aeronautics and Astronautics
Student Member AIAA

Introduction

The concept of aeroelastic tailoring has renewed the interest in forward swept wings, and consequently this configuration has been the focus of much of the research on the subject. The recent survey paper by Shirk et. al.[1] cites many studies of aircraft with forward swept wings, but relatively few dealing with high aspect ratio aft swept configurations. This is quite understandable since the first application of the concept was for the elimination of divergence of forward swept wings[2]. Weisshaar and Ryan[3] considered the effects of tailoring both forward and aft swept wings, but in quite a general manner.

However, future transport aircraft are certain to make use of composite materials in their primary structures, and are likely to have quite high aspect ratios[4]. A high aspect ratio aft swept wing is less prone to aeroelastic divergence, but the increase in aspect ratio could cause flutter to become a problem. One of the few papers devoted solely to the problem of tailoring high aspect ratio composite wings was the work by Gimmestad[5], but this was limited to some simple cases. A further area of aeroelastic tailoring that has received relatively little attention is in the use of non-symmetric laminates. This research considers the use of both symmetric and non-symmetric laminates to improve the aeroelastic performance of high aspect ratio, aft-swept wings.

This problem is solved using an integrating matrix method, which was used by Lehman[6,7] to analyse some simple aeroelastic examples, and by Green[8] to study the effects of stores on forward swept wings. The method requires the fourth order differential equation for flutter to be written in a state vector form, and then an integrating matrix is applied to the resulting first order matrix equation, which is then solved iteratively. Although this is a numerical solution method, it requires only a small number of elements (typically four or five) to obtain a converged solution. The main advantage of the integrating matrix method is that, since it only requires a small number of elements, a large number of parameters can be investigated. Clearly the choice of layup of the fibres is fundamental to the design process, and this forms the bulk of the research. Other parameters, such as aspect ratio and taper ratio are also investigated.

Solution of the Aeroelastic Equations

State Vector Formulation

The aeroelastic behaviour of the wing shown in figure 1 may be represented as a fourth order differential equation, and the integrating matrix technique is applied to this equation to obtain a solution. An outline of the general method is given here, and a more detailed treatment is to be found in ref. 7.

In order to apply the integrating matrix method, the equation of motion must first be written in a state vector form. The fourth order differential equation is written in terms of a state vector comprised of four displacement
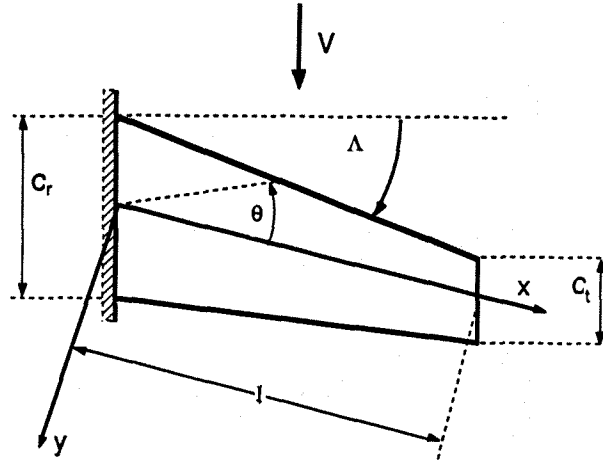

Figure 1. Geometric Layout of Wing

and four force degrees of freedom,

$$\frac{d}{dx}\begin{Bmatrix} N_x \\ M_x \\ V_x \\ M_{xy} \\ u \\ \gamma \\ w \\ \alpha \end{Bmatrix} = \begin{bmatrix} 0 & 0 & 0 & 0 & 0 & 0 & 0 & 0 \\ 0 & 0 & 1 & 0 & 0 & 0 & 0 & 0 \\ 0 & 0 & 0 & 0 & 0 & 0 & 0 & 0 \\ 0 & 0 & 0 & 0 & 0 & 0 & 0 & 0 \\ a_{11} & b_{11} & 0 & b_{13} & 0 & 0 & 0 & 0 \\ b_{13} & d_{11} & 0 & d_{13} & 0 & 0 & 0 & 0 \\ 0 & 0 & 0 & 0 & 0 & -1 & 0 & 0 \\ b_{13} & d_{13} & 0 & d_{33} & 0 & 0 & 0 & 0 \end{bmatrix} \begin{Bmatrix} N_x \\ M_x \\ V_x \\ M_{xy} \\ u \\ \gamma \\ w \\ \alpha \end{Bmatrix}$$

$$+ s^2 \begin{bmatrix} 0 & 0 & 0 & 0 & 0 & 0 & 0 & 0 \\ 0 & 0 & 0 & 0 & 0 & 0 & 0 & 0 \\ 0 & 0 & 0 & 0 & 0 & 0 & m_{ww} & m_{w\alpha} \\ 0 & 0 & 0 & 0 & 0 & 0 & m_{w\alpha} & m_{\alpha\alpha} \\ 0 & 0 & 0 & 0 & 0 & 0 & 0 & 0 \\ 0 & 0 & 0 & 0 & 0 & 0 & 0 & 0 \\ 0 & 0 & 0 & 0 & 0 & 0 & 0 & 0 \\ 0 & 0 & 0 & 0 & 0 & 0 & 0 & 0 \end{bmatrix} \begin{Bmatrix} N_x \\ M_x \\ V_x \\ M_{xy} \\ u \\ \gamma \\ w \\ \alpha \end{Bmatrix}$$

$$- \begin{bmatrix} 0 & 0 & 0 & 0 & 0 & 0 & 0 & 0 \\ 0 & 0 & 0 & 0 & 0 & 0 & 0 & 0 \\ 0 & 0 & 0 & 0 & 0 & L_\gamma & L_w & L_\alpha \\ 0 & 0 & 0 & 0 & 0 & M_\gamma & M_w & M_\alpha \\ 0 & 0 & 0 & 0 & 0 & 0 & 0 & 0 \\ 0 & 0 & 0 & 0 & 0 & 0 & 0 & 0 \\ 0 & 0 & 0 & 0 & 0 & 0 & 0 & 0 \\ 0 & 0 & 0 & 0 & 0 & 0 & 0 & 0 \end{bmatrix} \begin{Bmatrix} N_x \\ M_x \\ V_x \\ M_{xy} \\ u \\ \gamma \\ w \\ \alpha \end{Bmatrix}$$

$$(1)$$

or,

$$y' = Zy + s^2 My - Q(s,q)y \qquad (2)$$

The structural matrix Z is derived from an anisotropic plate beam model[9], and contains the compliances that are required for bending, torsion, and extension of a beam. The compliances are computed from the inverse of the modulus matrix, for which the moduli are given by,

$$A_{ij} = \int_{-h/2}^{h/2} Q_{ij} dz = h_0 \sum_{r=1-n/2}^{n/2} Q_{ij}^r [r - (r-1)]$$

$$B_{ij} = \int_{-h/2}^{h/2} Q_{ij} z \, dz = \frac{h_0^2}{2} \sum_{r=1-n/2}^{n/2} Q_{ij}^r [r^2 - (r-1)^2] \qquad (3)$$

$$D_{ij} = \int_{-h/2}^{h/2} Q_{ij} z^2 dz = \frac{h_0^3}{3} \sum_{r=1-n/2}^{n/2} Q_{ij}^r [r^3 - (r-1)^3]$$

1152

The terms Q_{ij} are the transformed moduli for each lamina and are dependent on the fibre orientation angle θ. These moduli are then integrated through the laminate, and if all layers have the same thickness (h_0) the integration is replaced by the sum shown in equation (3). It should be noted that if the lamina are arranged symmetrically with respect to the mid–line, there is no contribution to the B_{ij} terms, which can be dropped from the analysis. In such a case the N_x and u terms may be omitted, and this reduces the order of the system from 8×8 to 6×6. The following development describes the non–symmetric case, and the development using the reduced order system is found in reference 8.

The aerodynamic matrix Q is derived from modified strip theory[10], for which the time dependence is based on the Theodorsen function. The section lift curve slope may also be varied along the span.

Application of the Integrating Matrix

The integrating matrix technique is a numerical method which requires that the wing be discretised into $n-1$ elements with n nodes. Thus each term in the state vector, y, becomes a vector of order n, and the concept of a global state vector, $\hat{y}$, is introduced to represent the discretised version of the problem. Similarly, there will be global matrices $\hat{Z}$, $\hat{M}$, and $\hat{Q}$ comprised of $n \times n$ block diagonal matrices Z, M, and Q.

The global integrating matrix $\hat{L}$ is now defined as,

$$\hat{L} = \begin{bmatrix} L & \dots & 0 \\ \vdots & \ddots & \vdots \\ 0 & \dots & L \end{bmatrix} \qquad (4)$$

where L is the local integrating matrix. The local integrating matrix is in fact the product of a summing matrix S and a weighting matrix W_n,

$$L = S W_n \qquad (5)$$

The weighting matrices are based on Jacobi polynomials, and are given in ref. 7. The summing matrix S has the following form,

$$S = \begin{bmatrix} 1 & 0 & 0 & \dots & 0 \\ 1 & 1 & 0 & \dots & 0 \\ \vdots & \vdots & \vdots & \ddots & \vdots \\ 1 & 1 & 1 & \dots & 1 \end{bmatrix} \qquad (6)$$

and has dimensions $n \times n$.

$\hat{L}$ has the effect of integrating the derivative on the left hand side of equations (2) and (3),

$$\hat{L}\hat{y}' = \hat{y} \qquad (7)$$

and reducing the integration on the right hand side to simple matrix multiplication. Thus the integrated form of equation (2) is

$$\hat{y} = \hat{L}\hat{Z}\hat{y} + s^2\hat{L}\hat{M}\hat{y} - \hat{L}\hat{Q}(s,q)\hat{y} + \hat{k} \qquad (8)$$

It is also useful to write the equations in a more compact form by introducing the following definitions,

$$\hat{A} = s^2\hat{M} - \hat{Q}(s,q) \qquad (9)$$

where the contents of $\hat{A}$ can be derived from equation (1), and, for example,

$$A_{37} = s^2 m_{ww} - L_w \qquad (10)$$

Thus the integrated equation is

$$\hat{y} = \hat{L}\left[\hat{Z}\hat{y} + \hat{A}\hat{y}\right] + \hat{S}\hat{A}^+\hat{y} + \hat{k} \qquad (11)$$

where $\hat{k}$ is a vector of the constants of integration,

$$\hat{k} = \begin{bmatrix} k_{M_x} & k_V & k_{M_{xy}} & k_\gamma & k_w & k_\alpha \end{bmatrix}^T \qquad (12)$$

which are determined from the boundary conditions.

Boundary Conditions

The choice of boundary condition is of fundamental importance, for the condition applied affects both the complexity and accuracy of the solution. A cantilever condition is the simplest to apply, and was used in many of the early studies of aeroelastic tailoring. Although the use of such a condition precludes the detection of body freedom flutter[11,12], it is used here to avoid the appearance of non–homogeneous boundary condition terms.

It is first necessary to define a global boundary condition matrix $\hat{B}$ which has the following properties:

$$\hat{B}\hat{y} = 0 \qquad \hat{B}\hat{k} = \hat{k} \qquad (13)$$

This global matrix is once again made up of blocks of local boundary condition matrices, one for each of the variables. If both sides of equation (8) are multiplied by $\hat{B}$, and the properties of equation (13) are used, it is possible to solve for $\hat{k}$

$$\hat{k} = -\hat{B}\left[\hat{L}(\hat{Z}\hat{y} + \hat{A}\hat{y})\right] - \hat{B}_{nh}\hat{y} \qquad (14)$$

$\hat{B}_{nh}$ is a second boundary condition matrix which accounts for any non–homogeneous boundary conditions. This matrix is null for the cantilever case, but if rigid body modes are included it becomes non–zero, and this significantly complicates the solution.

Cantilever Boundary Condition

In general, a cantilever boundary condition requires that there be no displacement at the root and no force at the tip, thus

$$u(0) = 0 \qquad \gamma(0) = 0 \qquad w(0) = 0 \qquad \alpha(0) = 0 \quad (15)$$

$$N_x(0) = 0 \qquad M_x(1) = 0 \qquad V_x(1) = 0 \qquad M_{xy}(1) = 0 \qquad (16)$$

In order to apply these conditions it is necessary to expand equation (8) in terms of each variable, and then apply a local boundary condition. For purposes of illustration, the equation is expanded in terms of one variable at the tip (M_{xy}):

$$M_{xy} = L\left(A_{46}\gamma + A_{47}w + A_{48}\alpha\right) + k_{M_{xy}} \qquad (17)$$

1153

At the free end, $x = 1$, use is made of

$$\mathbf{b}_n^T = [0 \quad \cdots \quad 0 \quad 1]^T \tag{18}$$

having the following properties

$$\mathbf{b}_n^T \mathbf{M}_{xy} = M_{xy}(1) \qquad \mathbf{b}_n^T \mathbf{k}_{M_{xy}} = k_{M_{xy}} \tag{19}$$

Applying the boundary condition vector to equation (17) results in

$$\mathbf{k}_{M_{xy}} = -\mathbf{B}_n \Big[\mathbf{L} \left(\mathbf{A}_{34}\gamma + \mathbf{A}_{35}\mathbf{w} + \mathbf{A}_{36}\alpha \right) \Big] \tag{20}$$

Comparison with the appropriate part of equation (14) yields the local boundary condition matrix,

$$\mathbf{B}_{k_{M_{xy}}} = \vec{1}\mathbf{b}_n^T \equiv \mathbf{B}_n \tag{21}$$

Following a similar procedure for each of the other variables gives the global boundary condition matrix for the cantilever boundary condition

$$\hat{\mathbf{B}}_u = \begin{bmatrix} \mathbf{B}_n & 0 & 0 & 0 & 0 & 0 & 0 & 0 \\ 0 & \mathbf{B}_n & 0 & 0 & 0 & 0 & 0 & 0 \\ 0 & 0 & \mathbf{B}_n & 0 & 0 & 0 & 0 & 0 \\ 0 & 0 & 0 & \mathbf{B}_n & 0 & 0 & 0 & 0 \\ 0 & 0 & 0 & 0 & 0 & 0 & 0 & 0 \\ 0 & 0 & 0 & 0 & 0 & 0 & 0 & 0 \\ 0 & 0 & 0 & 0 & 0 & 0 & 0 & 0 \\ 0 & 0 & 0 & 0 & 0 & 0 & 0 & 0 \end{bmatrix} \tag{22}$$

If the laminate is symmetric, the boundary condition matrix is simply a reduced version of equation (22), so that the inclusion of the b_{ij} compliances does not influence the $\hat{\mathbf{B}}$ matrix. In the absence of non–homogeneous terms, $\hat{\mathbf{B}}_{nh} = 0$.

Equation Reduction

The problem is now in a position to be solved, since equation (14) can now be substituted into equation (8), and collecting terms allows the equation to be written as

$$\Big[\hat{\mathbf{H}} + \hat{\mathbf{P}}\hat{\mathbf{A}} \Big]\hat{\mathbf{y}} = 0 \tag{23}$$

where

$$\begin{aligned} \hat{\mathbf{P}} &= \Big[\hat{\mathbf{B}} - \hat{\mathbf{I}} \Big] \hat{\mathbf{L}} \\ \hat{\mathbf{H}} &= \Big[\hat{\mathbf{I}} + \hat{\mathbf{P}}\hat{\mathbf{Z}} + \hat{\mathbf{B}}_{nh} \Big] \end{aligned} \tag{24}$$

Since the state vector consists of force and displacement components, it can be written in partitioned form as

$$\left(\begin{bmatrix} \mathbf{H}_{FF} & 0 \\ \mathbf{H}_{DF} & \mathbf{H}_{DD} \end{bmatrix} + \begin{bmatrix} 0 & \mathbf{F}_{FF}\mathbf{A}_{FD} \\ 0 & 0 \end{bmatrix} \right) \begin{Bmatrix} \mathbf{y}_F \\ \mathbf{y}_D \end{Bmatrix} = \begin{Bmatrix} 0 \\ 0 \end{Bmatrix} \tag{25}$$

This equation can be solved simultaneously in order to eliminate the force variable $\mathbf{y}_F$, and this gives,

$$[\mathbf{I} + \mathbf{T}\mathbf{A}_{FD}]\mathbf{y}_D = 0 \tag{26}$$

where

$$\mathbf{T} = -\mathbf{H}_{DD}^{-1}\mathbf{H}_{DF}\mathbf{H}_{FF}^{-1}\mathbf{F}_{FF} \tag{27}$$

The matrix $\mathbf{T}$ contains structural information and information from the boundary conditions; $\mathbf{A}_{FD}$ contains aerodynamic and mass information about the wing; Since the problem is now written in terms of only half of the original state vector, the system of equations is reduced in size by a factor of four and solution is much faster.

The boundary condition matrix for the cantilever case is given by equation (22), and substitution of this into equation (24) allows analytical inversion of $\mathbf{H}_{DD}^{-1}$ and $\mathbf{H}_{FF}^{-1}$. This in turn permits analytic expressions for $\mathbf{T}$ to be formed:

$$\mathbf{T}_U = \begin{bmatrix} \mathbf{L}a_{11}\mathbf{L}_1 & \mathbf{L}b_{11}\mathbf{L}_1 & -\mathbf{L}b_{11}\mathbf{L}_1^2 & \mathbf{L}b_{13}\mathbf{L}_1 \\ \mathbf{L}b_{11}\mathbf{L}_1 & \mathbf{L}d_{11}\mathbf{L}_1 & -\mathbf{L}d_{11}\mathbf{L}_1^2 & \mathbf{L}d_{13}\mathbf{L}_1 \\ -\mathbf{L}^2b_{11}\mathbf{L}_1 & -\mathbf{L}^2d_{11}\mathbf{L}_1 & \mathbf{L}^2d_{11}\mathbf{L}_1^2 & -\mathbf{L}^2d_{13}\mathbf{L}_1 \\ \mathbf{L}b_{13}\mathbf{L}_1 & \mathbf{L}d_{13}\mathbf{L}_1 & -\mathbf{L}d_{13}\mathbf{L}_1^2 & \mathbf{L}d_{33}\mathbf{L}_1 \end{bmatrix} \tag{28}$$

For a symmetric laminate the matrix is slightly simplified.

$$\mathbf{T}_S = \begin{bmatrix} \mathbf{L}d_{11}\mathbf{L}_1 & -\mathbf{L}d_{11}\mathbf{L}_1^2 & \mathbf{L}d_{13}\mathbf{L}_1 \\ -\mathbf{L}^2d_{11}\mathbf{L}_1 & \mathbf{L}^2d_{11}\mathbf{L}_1^2 & -\mathbf{L}^2d_{13}\mathbf{L}_1 \\ \mathbf{L}d_{13}\mathbf{L}_1 & -\mathbf{L}d_{13}\mathbf{L}_1^2 & \mathbf{L}d_{33}\mathbf{L}_1 \end{bmatrix} \tag{29}$$

with

$$\mathbf{L}_1 = (\mathbf{B}_n - \mathbf{I})\mathbf{L} \tag{30}$$

Solution Procedure

Equation (26) has a solution if,

$$\det |\mathbf{I} + \mathbf{T}\mathbf{A}_{FD}(q, s)| = 0 \tag{31}$$

For each value of dynamic pressure q, equation (31) is solved iteratively to find the value of the Laplace variable s which makes the determinant zero. Muller's method[13] is an efficient root solving scheme that will find the roots of a complex matrix equation, and this is employed in the solution procedure.

One useful property of the cantilever boundary condition is that the $\mathbf{T}$ matrix is independent of both q and s, so for a particular wing geometry it can be evaluated before beginning the iteration procedure. This is not so when rigid body modes are included, because in that case $\mathbf{T}$ contains terms that depend on q and s. This requires that the matrix be recalculated for each iterate, and consequently increases the time needed for computational solution.

In order to determine the dynamic pressure at which aeroelastic instability occurs, the roots of equation (31) are traced out for increasing values of q until one of the roots crosses the imaginary axis. Thus a root locus in the s plane can be produced (fig. 2) which will indicate when an aeroelastic instability has occurred, and will also indicate whether it is flutter or divergence. If the vibration frequencies of the wing are also known and identified as being bending or torsion modes, it is possible to determine the type of flutter. The dimensionless flutter dynamic pressure shown in figure 2 is the reference flutter pressure which is used to normalise the remaining figures.
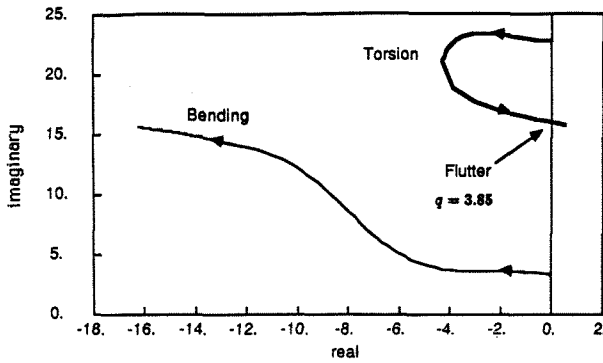
Figure 2. Root locus of reference flutter root:
$A.R. = 14$, $\Lambda = 0°$, $\theta = 0°$

It is not necessary to trace out a root locus for each configuration, and a procedure was implemented to find the dynamic pressure at which an instability occurs using a secant algorithm. This procedure locates the dynamic pressure at which the root locus crosses the imaginary axis, and indicates the type of aeroelastic instability.

Numerical Stability

As with any numerical method, some attention must be paid to stability or convergence. The choice of the number of nodes to be used is important for reasons of both speed and accuracy. As mentioned earlier, the size of the determinant to be solved is $3n \times 3n$ or $4n \times 4n$ and, since the determinant is solved iteratively, the speed at which the calculations are made is highly dependent upon the number of nodes.

Table 1

Number of nodes	Straight Wing	$r = 0.25$	Relative cpu time
4	4.158	16.66	0.39
5	4.164	17.20	0.63
5	4.164	17.24	1.00

Table 1 shows results for a straight wing and one with a taper ratio of 0.25. The number of nodes is varied from 4 to 6, and the relative computational time needed for solution using an IBM 3084 computer is shown. For the remaining results four nodes were used to keep computational time to a minimum. For the straight wing convergence is very good, even with four nodes, but when the wing is tapered six nodes are needed for the solution to converge. This is because the taper of the wing has to be treated in a discretised manner, and more nodes are needed to reflect the additional information. Since the purpose of this paper is to present more general trends, as opposed to a detailed analysis of a given configuration, the use of only four nodes is considered to be justified.

Results

The remainder of this analysis presents results for two different aspects of the problem. In the first part, geometric and aerodynamic effects are examined with a reference ply orientation. The integrating matrix method is shown to be capable of demonstrating the effects of both geometric and aerodynamic parameters, so that the geometry of the wing is not limited to a straight, untapered configuration with constant $C_{l\alpha}$. In the second part several different ply orientations, including non–symmetric laminates, are considered, and the effects of both ply orientation and modulus are shown.

In much of the literature on aeroelastic tailoring either the ply orientation or the modulus is given, but seldom both. An understanding of the effects of both are of importance to the designer, and so the results presented show the aeroelastic stability boundary as a function of a reference ply angle(θ), and also the dimensionless modulus as a function of the same ply angle. This allows the effect of ply angle on both stability and modulus to be considered. Following the lead of Weisshaar and Ryan[3], the moduli are made dimensionless in the following way:

$$R = \frac{D_{33}}{D_{11}} \qquad \psi = \frac{-D_{13}}{\sqrt{D_{11}D_{33}}}$$
$$\psi_1 = l\frac{B_{11}}{D_{11}} \qquad \psi_2 = l\frac{B_{13}}{D_{33}} \qquad (32)$$

The extensional coupling moduli need to be multiplied by a characteristic length, in this case the semi–span l, to become dimensionless. The use of the moduli in dimensionless form makes the results more general.

Geometric and Aerodynamic Effects

The design of an aircraft involves a large number of variables, and the use of composite materials increases the complexity of the design problem. The integrating matrix method is a useful tool for preliminary design work because it is not only fast, but also capable of modeling fairly sophisticated effects. In this section results are presented to show the effects of two geometric properties and one aerodynamic property. The properties of the wing common to all configurations are given in table 2.

Table 2

Structural	Material: AS/3501 Graphite Epoxy Number of Layers: 24 $e = -0.34$
Inertial	$m_\alpha = 1.0$ $\chi_\alpha = 0.2$ $r_\alpha = 0.538$
Aerodynamic	$a.c. = 0.25$ $\mu = 11.1$

The laminate code for all configurations in this section is given by

$$[\theta_1, \theta_2, 0, 0, \mp 45, 0, \mp 45, 0, \mp 45]_s \qquad (33)$$

where θ is the reference fibre orientation angle. For this first part of the study, the outermost plies on both top and bottom surfaces of the wing are varied as a group between $-50°$ and $50°$. The bending, torsional, and coupling moduli are shown in figure 3a, and the equivalent dimensionless parameters are shown in figure 3b.
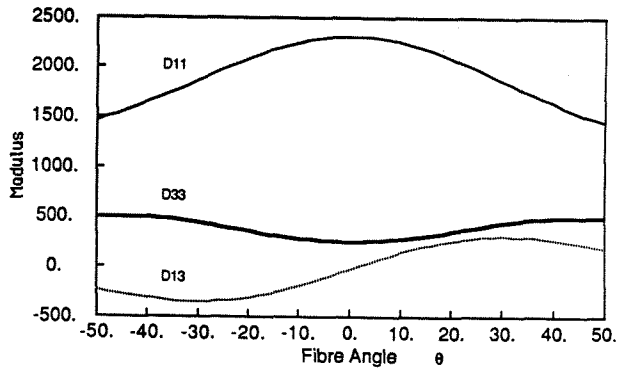
1155

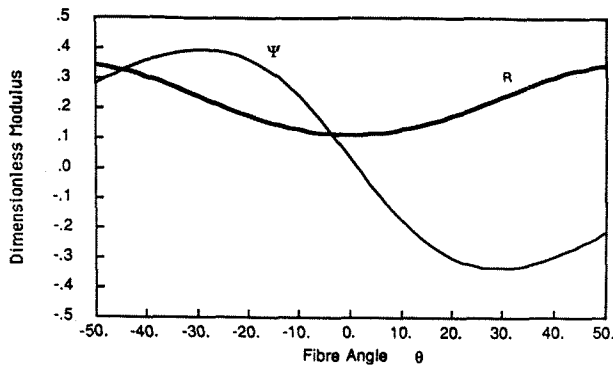**Figure 3a.** Dimensional moduli as a function of fibre angle θ for reference laminate

Figure 4. Aeroelastic stability boundary for: $A.R. = 10$ and $A.R. = 14$, $\Lambda = 10°$

Figure 3b. Dimensionless modulus parameters as a function of fibre angle θ for reference laminate
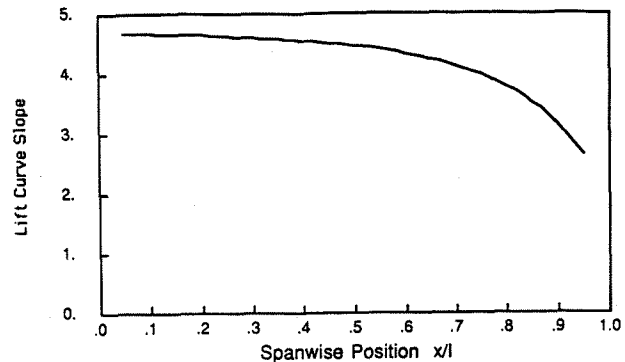
Figure 5. Lift distribution for wing with:

$A.R. = 14$, $\tau = 1.0$, $\Lambda = 0°$

Aspect Ratio

Most modern commercial aircraft are operating with aspect ratios in the range of 8 to 10, and their primary structure is aluminium. The next generation of such transport aircraft will make much more use of composite materials in their primary structure, and will be able to be designed with considerably higher aspect ratios. The study by Jensen et. al. [4] gives a number of designs optimised for various goals, for which the aspect ratios go up to 15, and wing sweep angles range between 10° and 40°.

One of the limitations on the maximum aspect ratio of a wing is structural, and the use of a composite wing structure offers advantages from both the structural and the aeroelastic viewpoint. Since the flutter speed of an aircraft decreases as the aspect ratio increases, in order to reach the proposed high aspect ratios the use of composites is mandated. By tailoring laminate it is possible to raise the flutter dynamic pressure over the equivalent quasi-isotropic value. Although it is not possible to eliminate the problem of flutter, the point may be reached where the aeroelastic benefits of increasing the flutter speed are off-set by the lowering of the bending stiffness of the wing.

Figure 4 shows the aeroelastic stability boundary for 10° swept wings of aspect ratio 10 and 14, and, as may
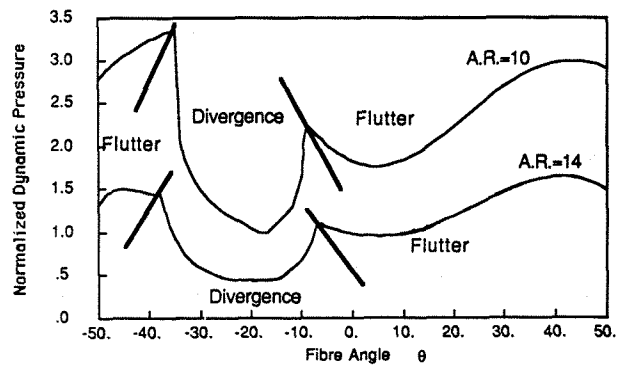
be anticipated, the lower aspect ratio wing has a higher boundary. By suitable tailoring it is possible to improve the performance of the $A.R. = 14$ wing so that its maximum flutter pressure is within 10% of the $\theta = 0$ pressure of the $A.R. = 10$ case. It may also be seen that when ψ is positive, divergence is the mode of instability. This is true for wings with lower sweep angles, but as will be shown as sweep increases divergence is completely avoided.

Lift Curve Slope

Modified strip theory allows some three dimensional aerodynamic effects to be included, and in this analysis the value of the lift curve slope $(C_{l\alpha})$ was either assumed constant, or calculated from LINAIR *, a computer programme based on the Weissinger method. As an example, the lift distribution of an aspect ratio 10 wing is shown in figure 5.

One disadvantage of chosing only four nodes is that the distribution of $C_{l\alpha}$ can only be represented in a crude fashion. When four nodes are used they are located at:

$$x = 0.0, \quad 0.276, \quad 0.724, \quad 1.0 \qquad (34)$$

This does not cause problems for a lift distribution as shown in figure 5, but would not be as good for a lift

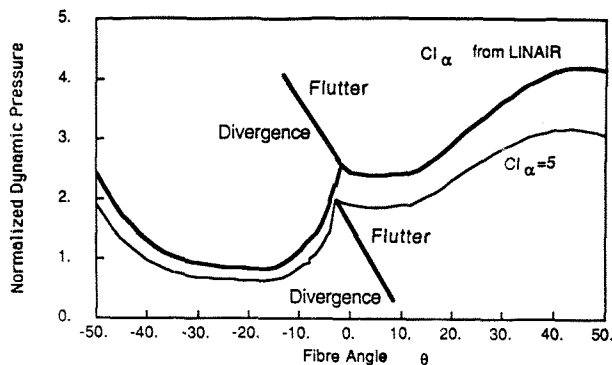* Developed by Prof. I. Kroo, Stanford University

1156

Figure 6. Effect of lift curve slope on aeroelastic behaviour:

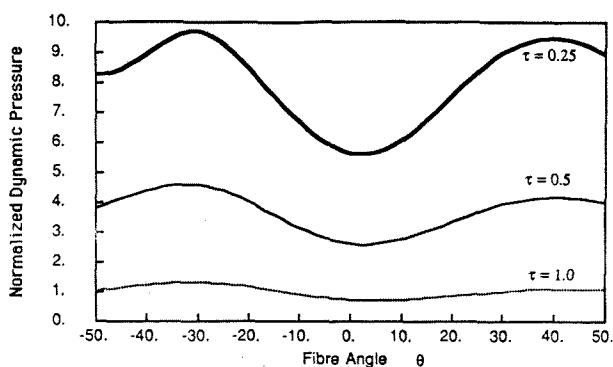$$A.R. = 10, \Lambda = 0°, \tau = 1.$$

Figure 7. Effect of taper ratio on aeroelastic behaviour:

$$A.R. = 10, \quad \Lambda = 30°, \quad C_{l\alpha} \text{ from LINAIR.}$$

distribution which had maximum lift close to mid–span, such as may occur with a highly swept wing.

Results are presented in figure 6 which show two different values of $C_{l\alpha}$ on an unswept, untapered wing of aspect ratio 10. When the lift curve slope is set to a constant value of 5, the stability boundary is more conservative than if the values of $C_{l\alpha}$ from figure 5 are used. The fibre angle at which the mode of instability changes from divergence to flutter is altered by only a few degrees, and again the trend is the same. Although the magnitude of the dynamic pressure is quite different for the two cases the shape of the curve is similar. For the unswept wing, divergence occurs over an even greater range of fibre angle.

Taper Ratio

Further refinement of the model is obtained when the wing is tapered. As shown in table 2, allowing the wing to be tapered slows down convergence and necessitates the use of more nodes. Results are shown in figure 7 which demonstrate the effects of a tapered plan–form of aspect ratio 10 with the lift curve slope calculated from LINAIR.

As the taper ratio is reduced, the flutter boundary is raised considerably due to a combination of improved aerodynamic loading for the tapered wings, and the reduction of the chord at the tip. This reduces the loads at the tip and thus raises the flutter speed. With the wing swept back 30° divergence has been eliminated for all values of ψ.

For trend studies such refinement may not be needed, but the method does have the capability to handle some fairly sophisticated details.

Aeroelastic Tailoring

Having considered some general trends with a fairly standard form of tailoring, some more interesting laminates are examined. Instead of just varying the two outermost plies together, treating them as a group, the outer laminae are varied separately, in both symmetric and non–symmetric layups.

Table 3

Structural	Material: AS/3501 Graphite Epoxy Number of Layers: 24 $e = -0.34$
Inertial	$m_\alpha = 1.0$ $\chi_\alpha = 0.2$ $r_\alpha = 0.538$
Aerodynamic	Aspect Ratio = 14 $c_{l\alpha} = 5.0$ $a.c. = 0.25$ $\mu = 11.1$

For the remaining results, the configuration used was an untapered wing of aspect ratio fourteen with a constant lift curve slope, as shown in table 3. Results are presented for several sweep angles, 0° and 10° which show the occurence of divergence, and 30° which is typical of all the moderately swept wings. These configurations were chosen to represent the high aspect ratio wings that may be used for future transport aircraft. The wing was not tapered and the lift curve slope was constant along the span, so the results are conservative. However, the trends shown could be expected to be unchanged if a more detailed aerodynamic model was chosen.

Symmetric Laminates

Twenty–four plies are used in all configurations, and the laminate code is,

$$[\theta_1, \theta_2, \theta_3, 0, \mp 45, 0, \mp 45, 0, \mp 45]_s \qquad (35)$$

In the previous section the tailoring was achieved by orienting plies θ_1 and θ_2 at the reference angle, and the results were not surprising, showing the optimum fibre angle to be around $-45°$ for cases when divergence was not a problem, and 45° when divergence was indicated. In order to see if any improvement could be obtained, and also to see if there were any laminates that should be avoided, some alternate patterns were tried.

Some improvement was seen when θ_2 was the reverse of θ_1, and this was due to the elimination of bending–torsion coupling. Figures 8a,b show the aeroelastic boundary and dimensionless modulus parameters
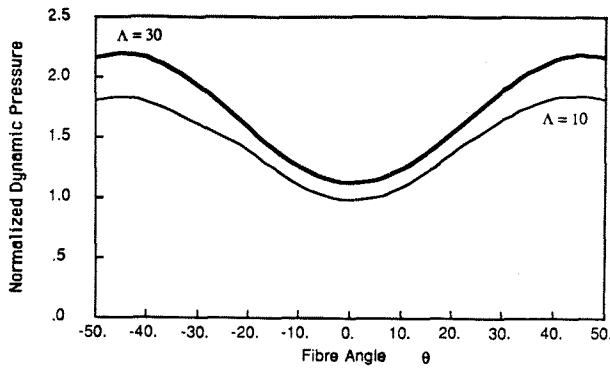
Figure 8a. Flutter boundary for:
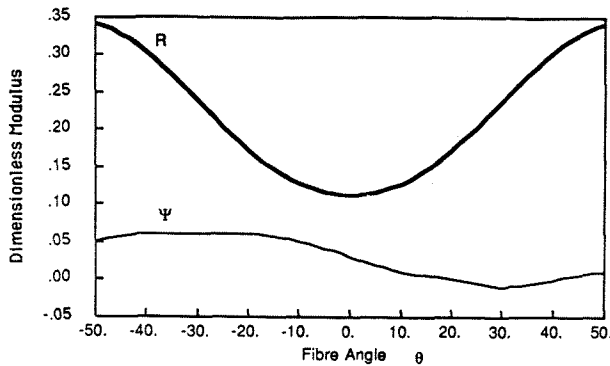
$$\theta_2 = -\theta_1.$$

Figure 8b. Dimensionless modulus parameters for:

$$\theta_2 = -\theta_1.$$

Figure 9a. Aeroelastic boundary for:

$$\theta_2 = \theta_1, \theta_3 = -\theta_1.$$
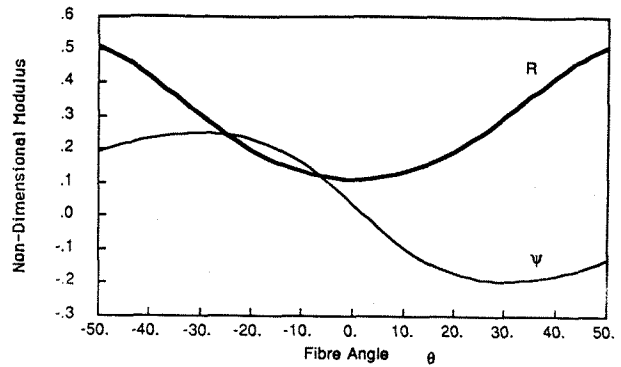
Figure 9b. Dimensionless modulus parameters for:

$$\theta_2 = \theta_1, \theta_3 = -\theta_1.$$

for this layup. Comparison of the 10° curve with that shown in figure 4 shows that divergence has been prevented, and the flutter boundary has been raised by about 10% when the plies are laid up at 45°. Divergence is prevented in this cases because the coupling parameter ψ is close to zero.

Further improvement was found when the third lamina was also varied, and figure 9a shows the stability boundary for this case with $\theta_2 = \theta_1$ and $\theta_3 = -\theta_1$. There is considerable improvement due to the increase in torsional stiffness, the maximum value of R is raised by about 30%, but since the laminate is no longer balanced there is some bending-torsion coupling. The increase in R raises the maximum flutter speed by 27% for the 30° swept wing, and by 22% for the unswept case. Since there is strong coupling, divergence reappears for the unswept case when ψ is negative.

Clearly this trend could be continued, ending with a laminate consisting of only ±45° laminae. This would, however, result in a wing that is very weak in bending which would not meet strength requirements. Thus the designer must reach a balance between the necessary bending stiffness and the aeroelastic constraints.
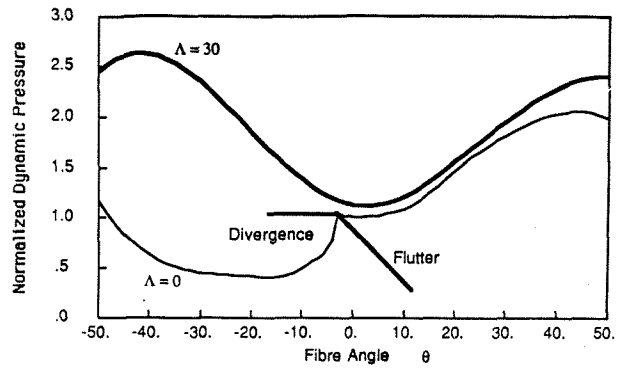
General Laminates

Symmetric laminates have a number of advantages over general, or non-symmetric, laminates. Firstly there is no warping of the laminate, and secondly they are easier to analyse, and offer fewer design decisions. However, general laminates should not be ignored simply because they complicate the problem; indeed, they give the designer the fullest benefit of an anisotropic material. Warping may be most problematical if flat panels are needed, since the warping may put initial stress in the laminate. If, however, the panel needs to be curved, such as may be the case for an aircraft wing, then using a non-symmetric laminate may offer the means to such curvature.

A number of non-symmetric laminates were examined, all having the following laminate code,

$$[\theta_1, \theta_2, 0, 0, \mp45, 0, \mp45, 0, \mp45, \\ \pm 45, 0, \pm45, 0, \pm45, 0, 0, \theta_{23}, \theta_{24}]_T \tag{36}$$

For general laminates two additional moduli, ψ_1 and ψ_2, are needed to define the structural behaviour of the wing. A laminate that has a ply at angle θ below the mid-plane and one with the same angle, positive or negative, at the same distance above the mid-plane, is said to be balanced, and has $B_{11} = \psi_1 = 0$.
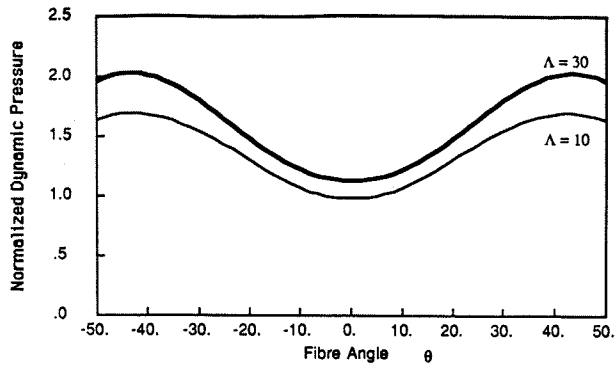
Figure 10a. Aeroelastic boundary for balanced general laminate:

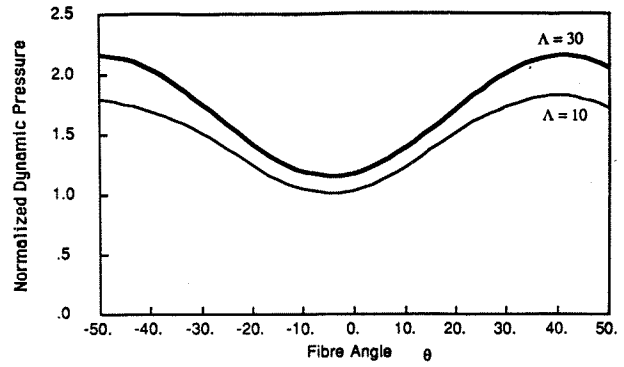$$\theta_1 = \theta_2 = -\theta \qquad \theta_{23} = \theta_{24} = \theta.$$

Figure 10b. Dimensionless modulus parameters R and ψ

Figure 10c. Dimensionless modulus parameters ψ_1 and ψ_3
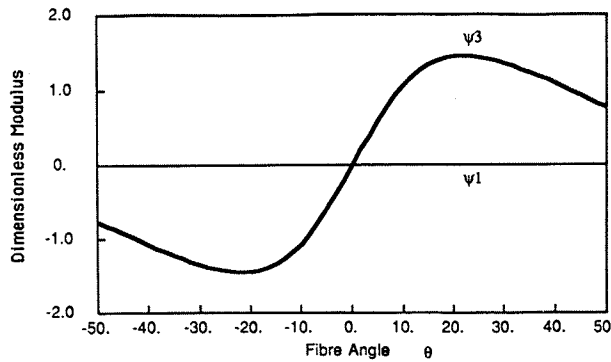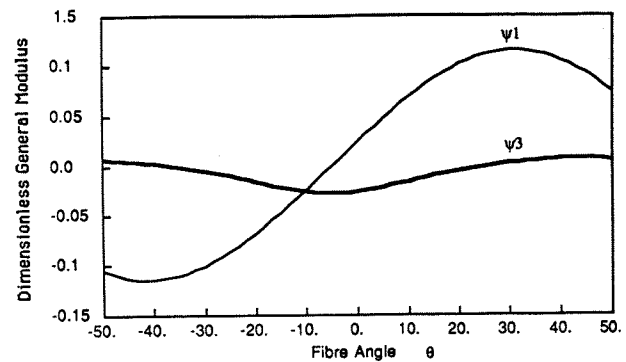
Figures 10a,b,c show the stability boundary and modulus curves for a balanced non–symmetric laminate, which is obtained by setting

$$\theta_1 = \theta_2 = -\theta \qquad \theta_{23} = \theta_{24} = \theta \qquad (37)$$

There is also little bending torsion coupling, $\psi \approx 0$, but there is strong extension–bending coupling.

Figure 11a. Aeroelastic boundary for unbalanced general laminate:

$$\theta_1 = \theta + 10°, \quad \theta_2 = \theta - 10°, \quad \theta_{23} = -\theta, \quad \theta_{24} = \theta.$$

Figure 11b. Dimensionless modulus parameters R and ψ

Figure 11c. Dimensionless modulus parameters ψ_1 and ψ_3

R and ψ are almost the same as in figure 8b, but the flutter maximum is lowered by about 7%. The results are still better than the reference laminate, but there is a penalty for having extension–torsion coupling.

The next laminate examined had the following layup,

$$\theta_1 = \theta + 10°, \quad \theta_2 = \theta - 10°, \quad \theta_{23} = -\theta, \quad \theta_{24} = \theta \qquad (38)$$
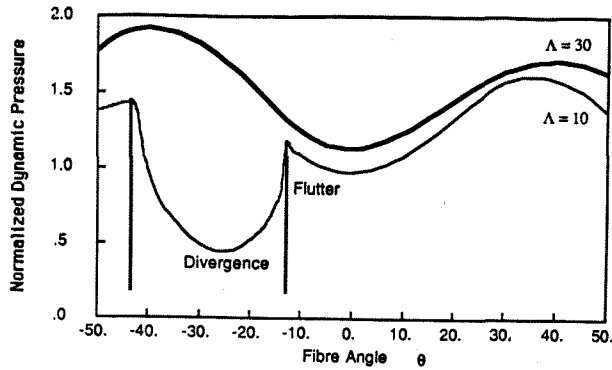
Figure 12a. Aeroelastic boundary for unbalanced general laminate:
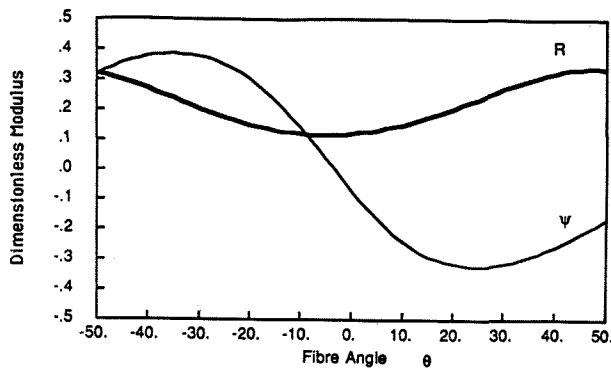$$\theta_1 = \theta_2 = \theta + 10°, \quad \theta_{23} = \theta_{24} = \theta.$$

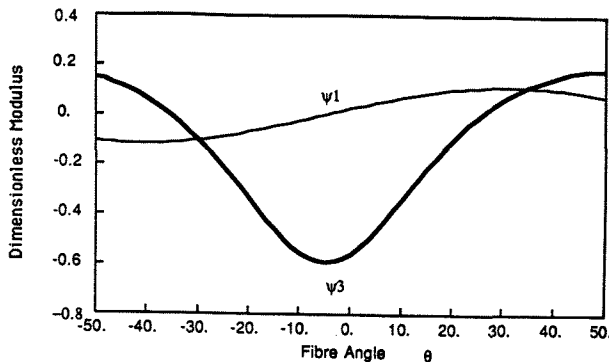**Figure 12b.** Dimensionless modulus parameters R and ψ

Figure 12c. Dimensionless modulus parameters ψ_1 and ψ_3

which had the effect of eliminating ψ and ψ_3, but allowing extension–bending coupling. The effect on the flutter boundary was to improve it to the point where the maximum flutter pressure was about the same as that of the symmetric laminate shown in figure 8a, and better than the balanced laminate of figure 10a.

As a final example, a completely general laminate was examined for which all three coupling parameters

were non–zero. The laminate used is described by equation (39):

$$\theta_1 = \theta_2 = \theta + 10°, \quad \theta_{23} = \theta_{24} = \theta \quad (39)$$

and the results are shown in figure 12. Since ψ is no longer zero, the 10° swept wing is again prone to divergence, and the maximum flutter pressures are almost the same as those for the reference laminate. Again there is some penalty for allowing coupling, but it need not prevent completely general laminates from being considered. The penalty for this case is partly due to the extensional coupling, and partly due to the reappearance of bending–torsion coupling.

Conclusions

The aim of this analysis was to examine the usefulness of the integrating matrix method for the study of the aeroelastic stability for fairly arbitrary geometries, and to examine the possibilities of using general, non-symmetric, laminates.

When using the integrating matrix method it is possible to analyse the aeroelastic behaviour of wings in some detail. Although there is some penalty in terms of computational time needed, tapered geometries present no difficulty. The aerodynamic characteristics of the problem can also be improved by calculating the lift curve slope from a Weissinger type method. This again adds time to the analysis, but indicates that the method may be suitable for quite detailed designs.

Most studies in aeroelastic tailoring have considered only symmetric laminates, but it is of interest to see what effect the use of a general laminate has. Non–symmetric laminates introduce two additional coupling parameters to the problem, and three general laminates were examined to reflect the contribution of each of these on the stability. Extension–torsion coupling, ψ_3, caused some degradation of the flutter boundary; extension–bending coupling, ψ_1, was not as damaging as ψ_3, and gave a flutter boundary that was as good as the best symmetric laminate with the same torsion–bending stiffness ratio. When both ψ_1 and ψ_3 were present, the performance of the wing was degraded to that of the symmetric reference laminate.

It was only possible to examine a limited number of laminates, and if general laminates are to be used there are even more permutations to add to the designers problem. However, this preliminary investigation shows that there need not be a severe penalty for making use of a general laminate, and this is a topic worthy of further research.

References

1 Shirk, M. H., Hertz, T. J., Weisshaar, T. A., "Aeroelastic Tailoring-Theory, Practice and Promise," *Journal of Aircraft*, Vol. 23, No. 1, January 1986.

2 Krone, N. J., "Divergence Elimination with Advanced Composites," AIAA Paper 75–1009, August 1975.

3 Weisshaar, T. A. and Ryan, R. J., "Control of Aeroelastic Instabilities through Stiffness Cross Coupling," *Journal of Aircraft*, Vol. 23, No. 2, Feb. 1986.

4 Jensen, S. C., Rettie, I. H., and Barber, E. A., "Role of Figures of Merit in Design Optimization and Technology Assessment," AIAA Paper 79-0234R, Feb. 1981.

5 Gimmestad, D., "An Aeroelastic Optimization Procedure for Composite High Aspect Ratio Wings," AIAA Paper 79-0726, 1979.

6 Lehman, L. L., "A Hybrid State Vector Approach to Aeroelastic Analysis with Applications to Composite Lifting Surfaces," AIAA Paper 81-0626, April 1981.

7 Lehman, L. L., "Hybrid State Vector Methods for Structural Dynamic and Aeroelastic Boundary Value Problems," Ph. D. Thesis, Stanford University, Stanford, CA, February 1982.

8 Green, J. A., "Aeroelastic Tailoring of Composite Wings with External Stores," AIAA Paper 86-1021-CP, May 1986.

9 Tsai, S. W., and Hahn, H. T., *Introduction to Composite Materials*, Technomic Publishing Company, 1980.

10 Yates, E. C., Jr., "Flutter and Unsteady Lift Theory. Performance of Aerospace Vehicles," NASA SP 258, 1971.

11 Weisshaar, T. A., Zeiler, T. A., Hertz, T.J., and Shirk, M. H., "Flutter of Forward Swept Wings, Analyses and Tests," AIAA Paper 82-0646, May 1982.

12 Chen, G-S. and Dugundji, J.,"Experimental Aeroelastic Behavior of Forward Swept Graphite/Epoxy Wings with Rigid Body Freedoms," AIAA Paper , May 1986.

13 Conte, S., D. and deBoor, C., *Elementary Numerical Analysis. An Algorithmic Approach*, 2nd. ed., McGraw-Hill, New York, 1972.